Consequences of Binding an *S*-Adenosylmethionine Analogue on the Structure and Dynamics of the Thiopurine Methyltransferase Protein Backbone†

Thomas H. Scheuermann,‡ Camille Keeler,§ and Michael E. Hodsdon*,§

Departments of Molecular Biophysics and Biochemistry and of Laboratory Medicine, Yale University, New Haven, Connecticut 06520

Received April 14, 2004; Revised Manuscript Received July 15, 2004

ABSTRACT: In humans, the enzyme thiopurine methyltransferase (TPMT) metabolizes 6-thiopurine (6-TP) medications, commonly used for immune suppression and for the treatment of hematopoietic malignancies. Genetic polymorphisms in the TPMT protein sequence accelerate intracellular degradation of the enzyme through an ubiquitylation and proteasomal-dependent pathway. Research has led to the hypothesis that these polymorphisms destabilize the native structure of TPMT, resulting in the formation of misfolded or partially unfolded states, which are subsequently recognized for intracellular degradation. Addition of the cosubstrate, *S*-adenosylmethionine (SAM), prevents degradation of the TPMT polymorphs in experimental assays, presumably by stabilizing the native structure. Using a bacterial orthologue of TPMT from *Pseudomonas syringae*, we have used NMR spectroscopy to describe the consequences of binding sinefungin, a SAM analogue, on the structure and dynamics of the TPMT protein backbone. NMR chemical shift mapping experiments localize sinefungin to a highly conserved site in classical methyltransferases. Distal chemical shift changes involving the presumed active site cover imply *indirect* conformational changes induced by sinefungin, which may play a role in substrate recognition or the catalytic mechanism. Analysis of protein backbone dynamics based on NMR relaxation reveals a combination of complementary effects. Whereas the peripheral, inserted structural elements of the TPMT topology are conformationally stabilized by the presence of sinefungin, a consistent increase in backbone mobility is observed for the central, conserved structural elements. The potential implications for the structural and dynamic effects of binding sinefungin for the catalytic mechanism of the enzyme and the stabilization of the degradation-susceptible TPMT polymorphs are discussed.

While the endogenous function of human thiopurine methyltransferase (TPMT)[1] is not well understood, it has long been recognized for catalyzing the *S*-adenosylmethionine-(SAM-) dependent S-methylation of 6-thiopurine (6-TP) medications (*1*−*3*). These drugs are commonly utilized for immune suppression and in the treatment of childhood acute lymphoblastic leukemia. Azathioprine, 6-thioguanine, and 6-mercaptopurine are prodrugs, being converted by familiar metabolic machinery into 6-thioguanine nucleotides (6-TGNs), which trigger programmed cell death when incorporated into DNA. S-Methylation by TPMT diverts these compounds from their route of efficacy, effectively inactivating a portion of the administered dose. Interindividual heterogeneity in tissue TPMT activities complicates the administration of 6-TP medications by varying their conversion into active 6-TGNs. Allelic polymorphisms in the TPMT gene responsible for this heterogeneity have been identified and primarily result in single or double amino acid substitutions in the TPMT protein sequence. Approximately 1 in every 300 persons is homozygous for the polymorphic alleles and is nearly completely deficient in the enzyme (*4*), putting them at high risk for life-threatening myelosuppression from standard doses of 6-TP medications. Heterozygotes, representing 10% of the population, have intermediate levels of activity and suffer from an increased risk of 6-TP drug toxicity. As a consequence of these clear associations, 6-TP dosage adjustments have been defined on the basis of a patient's TPMT genotype, representing one of the first major successes for the expanding field of pharmacogenetics (*5*, *6*).

The biochemical basis for the significant deficiency in tissue enzyme activity associated with the most common TPMT alleles has been extensively investigated. Decreased TPMT activity measured in tissues correlates with decreased levels of the TPMT protein, suggesting that the polymorphisms of the protein sequence do not simply affect the catalytic function of the enzyme (*7*). Instead, subsequent studies have firmly established that the decreased steady-state level of TPMT polymorphs is the result of increased

† This work was supported by National Institutes of Health Grant K08-AI01806 (M.E.H.) and by a Biomedical Research Grant from the National Blood Foundation (M.E.H.).

* To whom correspondence should be addressed. Phone: 203-737-2674. Fax: 203-688-3725. E-mail: michael.hodsdon@yale.edu.

‡ Department of Molecular Biophysics and Biochemistry, Yale University.

§ Department of Laboratory Medicine, Yale University.

[1] Abbreviations: TPMT, thiopurine methyltransferase; SAM, *S*-adenosylmethionine; 6-TP, 6-thiopurine; 6-TGN, 6-thioguanine nucleotide; 6-MP, 6-mercaptopurine; psTPMT, *Pseudomonas syringae* TPMT; GST, glutathione *S*-transferase; IPTG, isopropyl thiogalactopyranoside; PFG, pulsed field gradients; 3D, three dimensional; CSI, chemical shift index; MUP-1, major urinary protein-1; DHFR, dihydrofolate reductase; hsp90, heat shock protein 90.

10.1021/bi0492556 CCC: $27.50
Published on Web 08/31/2004

degradation of the enzyme, most likely through an ubiquitylation and proteasomal-dependent pathway (*8*, *9*). Recent work has revealed the involvement of the molecular chaperone hsp90 in the folding and degradation of TPMT polymorphs (*10*). While hsp90 is best known for its role in protein refolding, it is presently understood to act as a molecular switch that also directs misfolded proteins to pathways for intracellular degradation. Nascent TPMT polypeptide chains utilize hsp90 to properly fold, and the common, degradation-resistant variant of the protein is rapidly released from the chaperone after efficiently achieving a stable conformation. On the other hand, the clinically significant, degradation-susceptible polymorphs appear less amenable to hsp90-mediated refolding, possibly requiring multiple catalytic cycles and thus permitting sufficient time for the recruitment of degradation-promoting cofactors directing the polymorphs to ubiquitylation and proteasomal degradation.

The above research has led to a central hypothesis that genetic polymorphisms in the TPMT protein sequence destabilize the native state of the protein and shift the ensemble of conformations in aqueous solution toward misfolded or partially destabilized states, which are subsequently recognized by the above machinery for intracellular degradation. Support for this hypothesis is provided by the observed inhibition of TPMT polymorph degradation by the addition of SAM, a cosubstrate and high-affinity ligand for TPMT, to experimental assays of protein degradation (*8*, *9*). Ligand binding to the TPMT polymorphs would be thermodynamically linked to protein folding and would be expected to stabilize the native state, thus avoiding prolonged interaction with the hsp90 chaperone and subsequent targeting for intracellular degradation. As the first step of a long-term effort to uncover the structural mechanism for polymorphic destabilization of the TPMT tertiary structure, we undertook to describe the structural consequences of binding SAM to the protein. However, as SAM is chemically unstable in aqueous solution, the SAM analogue and general methyltransferase inhibitor, sinefungin, was utilized as a surrogate. This choice is justified by the high chemical similarity of the two compounds (see Supporting Information) and the widespread use of sinefungin in many previous crystallographic studies of SAM-dependent methyltransferases (*11*), where no significant differences are noted in tertiary structures with either SAM or sinefungin bound to the same enzyme.

Due to difficulties with aggregation of human TPMT at high concentrations, we previously used NMR spectroscopy to determine the tertiary structure of a bacterial TPMT orthologue in its unliganded state (*12*) [presented in Figure 1, generated using MOLMOL (*13*)]. Originally identified as a genetic determinant of tellurite resistance in *Pseudomonas syringae*, the bacterial orthologue shares 45% similarity (33% identity) with the human protein and similarly acts as a SAM-dependent methyltransferase for 6-TPs (*14*). Initial studies revealed an unstructured N-terminus, which was removed for structural studies and subsequently determined to be required for enzymatic activity. The tertiary structure of bacterial TPMT reveals a classical SAM-dependent methyltransferase topology (*11*) (see Figure 1), consisting of a seven-stranded β-sheet flanked by α-helices on both sides. However, some deviations from the consensus topology

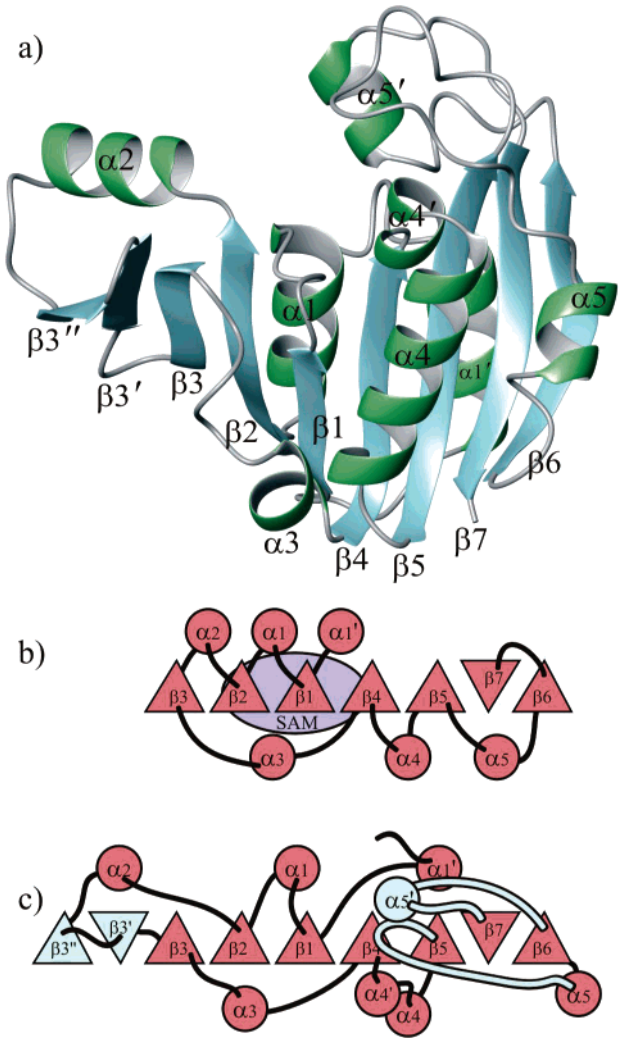

FIGURE 1: Backbone ribbon diagram (a) of the psTPMT tertiary structure along with a consensus topology for the conserved family of classical methyltransferases (b) compared to the topology of psTPMT (c). Triangles and circles denote β-strands and α-helices, respectively, with the relative orientation of β-strands indicated by rotation of the triangles. The approximate, conserved binding site for *S*-adenosylmethionine (SAM) is illustrated in violet. Secondary structural elements that are conserved in the consensus methyltransferase toplogy are colored light red, whereas the structural insertions in the psTPMT topology are colored cyan. All tertiary structures in this and the remaining figures were generated using MOLMOL (*13*).

along with multiple insertions of structural elements are evident, including a novel pair of antiparallel β-strands present between α2 and β3. A review of the many experimentally determined tertiary structures of small molecule methyltransferases demonstrates that such structural deviations from the consensus topology are common and found in similar locations. An important set of structural elements are typically observed covering the substrate recognition site and the catalytic center of the enzymes, which is frequently referred to as the "active site cover". In psTPMT(Δ17), two extended loops inserted between β5−α5 and β6−β7 are responsible for creating this structural feature, which includes the α5′ helix.

In the current study, we build upon our previous results by describing the structural consequences of binding sinefungin on the structural properties of psTPMT(Δ17). The SAM−sinefungin recognition site is approximately localized

based upon NMR chemical shift mapping and found to correspond to a highly conserved location in the family of classical methyltransferases. The consequences of ligand binding on the dynamics of the polypeptide backbone, as described using a model-free analysis of NMR relaxation, are dramatic. Whereas the peripheral, inserted structural elements of the psTPMT(Δ17) topology were conformationally stabilized by the presence of sinefungin, a uniform increase in backbone mobility was identified in the central, conserved structural elements. The implications for an increase in structural flexibility in the ligated states of the degradation-susceptible TPMT polymorphs by SAM are discussed. A combination of changes in backbone mobility and chemical shifts stretching from the active site cover to distal portions of the psTPMT(Δ17) tertiary structure involving conserved residues are speculated to play a role in catalysis, based upon similar findings in dihydrofolate reductase. Lastly, as these results represent the first description of the solution-state backbone dynamics for a classical SAM-dependent methyltransferase and given the high degree of structural conservation within this protein family, we speculate on a general role for these structural and dynamic effects of SAM−sinefungin binding in the function of related small molecule methyltransferases.

EXPERIMENTAL PROCEDURES

Sample Preparation. The N-terminal deletion mutant, psTPMT(Δ17), lacking the first 17 residues of the *P. syringae* TPMT sequence, was expressed and purified as previously described (*12*). Briefly, protein was recombinantly expressed in BL21 *Escherichia coli* as a fusion protein with glutathione *S*-transferase (GST). Bacterial cultures were grown in isotope-enriched media (Spectra Gases), induced with 1 mM IPTG, and allowed to express protein overnight at room temperature. GST−psTPMT(Δ17) was purified from the soluble phase of the cell lysate with glutathione−Sepharose (Amersham Biosciences) and treated with thrombin (Amersham Biosciences) while still bound to the resin. After elution, psTPMT(Δ17) was exchanged into 20 mM potassium phosphate, pH 6.8, and 150 mM NaCl and its concentration quantified by UV absorption spectroscopy. Measurements of NMR relaxation were performed with 0.75 mM ^{15}N-labeled psTPMT and in the presence or absence of 7.5 mM sinefungin; all NMR samples contained the above solution conditions along with 5% D_2O, 0.05% sodium azide, 20 μM DSS (Fluka), and 10 μM each of the protease inhibitors PMSF (Sigma) and leupeptin and pepstatin (Calbiochem).

NMR Resonance Assignments. All NMR experiments were collected at 20 °C on a Varian INOVA 600 MHz spectrometer with a 5 mm triple resonance (HCN) probe equipped with triple axis (XYZ) pulsed magnetic field gradients (PFGs) and employing pulse sequences available in the Varian BioPack user library (Varian Inc., Palo Alto, CA). Resonance assignments of ^{13}C,^{15}N-labeled psTPMT(Δ17)−sinefungin were determined by manual analysis of three-dimensional (3D) HNCO, HNCA, HNCACB, HN(CO)CA, CBCA(CO)NH, (HCA)CO(CA)NH, CC(CO)NH, HCC(CO)-NH, and HCCH-TOCSY NMR experiments. Backbone chemical shift assignments for psTPMT(Δ17)−sinefungin were nearly complete with 184 out of 192 backbone amide, 196 out of 201 Cα, 179 out of 184 Cβ, and 193 out of 201 Hα resonances identified. Previously for apo psTPMT(Δ17), 190 out of 192 backbone amides, 199 out of 201 Cα, 183 out of 184 Cβ, and 194 out of 201 Hα resonances were assigned. Protein secondary structure was evaluated using the consensus chemical shift index (CSI) and a single 3D ^{15}N-NOESYHSQC NMR experiment collected with a 150 ms isotropic mixing time.

Titration of Sinefungin Binding Using NMR Spectroscopy. The interaction between sinefungin and psTPMT(Δ17) was monitored by changes in backbone amide ^{1}H and ^{15}N chemical shifts in a series of 2D ^{1}H−^{15}N HSQC spectra during a titration of sinefungin with a constant concentration of protein. Beginning with a 700 μL sample of 50 μM ^{15}N-labeled psTPMT, the sinefungin concentration was increased incrementally (0, 25, 50, 100, 150, 200, 250, 300, 400, and 500 μM) by sequential addition from a 10 mM sinefungin solution. To limit losses associated with sample transfer, a small quantity (approximately 50 μL) of the NMR sample was removed from the NMR tube via a long-stemmed glass pipet (Kontes), the appropriate small volume of sinefungin stock solution was added to this aliquot, and the resulting mixture was returned to the NMR tube, gently mixed with the glass pipet, and allowed to equilibrate for 20−30 min before acquisition of NMR spectra. Well-resolved peaks undergoing apparent fast exchange and experiencing significant chemical shift changes during the titration were selected for analysis (see representative examples in the Supporting Information). A total of 22 ^{1}H and ^{15}N chemical shifts were simultaneously fit to various models of ligand binding using the SigmaPlot (SPSS Inc., Chicago, IL) software package in order to estimate sinefungin binding affinity.

NMR Relaxation Measurements. Pulse sequences for measurement of NMR relaxation rates and the steady-state ^{1}H→^{15}N NOE incorporated sensitivity enhancement, water flip-back pulses, and coherence selection via PFGs (*15*). For determination of R_1 relaxation rates, NMR experiments were serially repeated with time delays of 100, 200, 300 (×2), 600, 800, 1000, 2000, and 3000 ms, and for determination of R_2, experiments were serially repeated with delays of 10, 30 (×2), 50, 70, 90, 130, 150, and 210 ms. The steady-state NOE experiment was performed with and without a 3 s saturation period to allow buildup of the NOE. Individual increments were separated by a 1 s recycle delay during determination of R_1 and R_2 relaxation rates, while the steady state ^{1}H→^{15}N NOE experiment used a total recycle delay of 6 s. Spectral widths of 9 and 2.1 kHz in the f_2 and f_1 dimensions were set in all experiments, with 128 transients collected per t_1 increment, and recorded as 256 complex t_1 values against 1024 complex t_2 values. All experiments were processed with NMRpipe (*16*) and inspected visually in Sparky (*17*).

Exponential Fitting of Relaxation Rates. NMR peak heights determined by the "rh" command in Sparky were used as reliable indicators of spectral intensity. The program "sparky2rate"[2] read in peak intensity tables from Sparky and acted as a front end for Curvefit,[3] for exponential fitting of R_1 and R_2 NMR relaxation rates and an analysis of their

[2] Available at http://xbeams.chem.yale.edu/~loria/software.htm.

[3] Available at http://cpmcnet.columbia.edu/dept/gsas/biochem/labs/palmer/software.html.

associated errors using Monte Carlo simulations, which depended upon an initial error estimated from the repeated experiments. Numerous residues were excluded from relaxation analysis on the basis of poor chemical shift dispersion [for apo psTPMT(Δ17), L26, D51, K92, Y94, R123, A124, V138, L144, S150, L152, and S180; for psTPMT(Δ17)−sinefungin, E21, L33, L45, K48, S49, A71, T86, Y121, L141, S197, R199, H211, and E216] or missing backbone amide resonance assignments [H18 and S49 for apo psTPMT(Δ17) and H18, Q19, S20, F106, A124, A125, M126, and A198 for psTPMT(Δ17)]. Appropriately, relaxation data are not reported for prolines (residues 37, 44, 83, 97, 130, 146, 166, 167, and 171).

Model-Free Analysis. Modelfree version 4.15 was used to calculate global and residue-specific motional parameters (*18*). The program FAST-Modelfree (*19*) automated the error analysis and model selection that otherwise requires frequent user input and intervention. An initial rotational correlation time (τ_m) was estimated from the 10% trimmed mean of the R_2/R_1 ratio. An appropriate diffusion tensor was selected by comparing the calculated optimal τ_m value and χ^2 error of simulations run under the assumption of isotropic or axially symmetric tumbling behavior. The isotropic condition was selected for both apo and liganded psTPMT(Δ17) as there were no differences in χ^2 or τ_m values associated with the two rotational models, and the best-fit values of the D_{ratio} for anisotropic rotation were not significantly different from unity. All model-free calculations were run with the CSA tensor set to −172 (*20*), a value considered appropriate for the ^{15}N spins of proteins and a backbone amide bond length of 1.00 Å, which had previously been used by CYANA for determination of the psTPMT(Δ17) tertiary structure (*12*).

Sequence Alignment. A multiple sequence alignment of TPMT orthologues was generated by ClustalW (*21*, *22*) with the following settings: opening and end gap penalties set to 10, the extending and separation gap penalties set to 0.05, and selection of the Blosum scoring matix. The ClustalW text-only output was rendered with the program Boxshade in order to graphically emphasize sequence conservation (available as Supporting Information). While various genomic intiatives have idenitified a large number of sequences highly similar to psTPMT, the vast majority of these putative TPMT orthologues has not been subjected to any further characterization. In this alignment we include five mammalian TPMT sequences and only those two bacterial sequences for which activity has been experimentally established (*14*, *23*, *24*): *Homo sapiens*, *Canis familiariz*, *Ratus norvegicus*, *Mus musculus*, *Mus spretus*, *P. syringae* and *Pseudomonas anguilliseptica*.

RESULTS

Selection of Stoichiometric Ratios of Sinefungin to psTPMT(Δ17) for NMR Experiments. The precise binding affinities for binding SAM or its analogue, sinefungin, to psTPMT(Δ17) have never been reported. Analyses of enzyme kinetics for full-length TPMTs (*25*) and for other methyltransferases (*26*−*32*) have revealed apparent Michaelis−Menten (K_m) constants for SAM and inhibitory (K_i) constants for sinefungin in the range of 1−500 μM. However, determination of their precise binding affinity is complicated by racemization at a chiral center (*33*−*35*). Only the *S*-stereoisomer of SAM is catalytically active for methyltransferases and, in aqueous solution, undergoes both a reversible conversion to the inactive *R*-stereoisomer and an irreversible hydrolysis to yield 5′-deoxy-5′-(methylthio)adenosine and homoserine. Sinefungin is considered stable in water, avoiding the complication of hydrolysis, but the consequences of sinefungin stereochemistry on methyltransferase binding are not known. We attempted to fit the chemical shift changes for 22 protein resonances in 2D ^{1}H−^{15}N HSQC NMR spectra to models of *N* identical binding sites and to a single class of sites (*N* fixed at 1). However, given the above uncertainty about the effects of sinefungin stereochemistry on binding (possibly each stereoisomer binds the protein with a different affinity), we are only comfortable in reporting that the titration results are generally consistent with an *apparent* dissociation constant in the range of 10−100 μM.

In the series of 2D ^{1}H−^{15}N HSQC NMR spectra collected during titration of sinefungin against a constant concentration of psTPMT(Δ17), variable degrees of spectral broadening are observed for a subset of residues at intermediate stoichiometric ratios, which is most likely a consequence of exchange rates between the liganded and unliganded states being on the order of the chemical shift differences (expressed in hertz) for the involved nuclei. In the presence of a high excess of sinefungin, the protein becomes saturated, and as the concentration of free ligand increases, the exchange rate becomes much greater than the chemical shift differences for all the nuclei and, consequently, their HSQC peaks return to a narrower line width (although some resonances apparently remain broadened independent of ligand concentration and are discussed further below). To ensure that exchange between ligation states does not complicate interpretation of the NMR relaxation experiments, a high stoichiometric ratio of 10:1 sinefungin:protein was chosen for analysis. Due to concern about the possibility of nonspecific association of sinefungin with the protein at these high stoichiometric ratios, the chemical shift mapping experiments were also performed at a relatively lower amount of sinefungin representing only a 10% excess of ligand.

Chemical Shift Comparison for Apo psTPMT(Δ17) and psTPMT(Δ17)−Sinefungin. Addition of the SAM-dependent methyltransferase inhibitor sinefungin significantly perturbs the NMR chemical shifts of psTPMT(Δ17), as illustrated by the comparison of 2D ^{1}H−^{15}N HSQC spectra in Figure 2. Chemical shift differences for backbone amide, Hα, Cα, and Cβ nuclei between apo psTPMT(Δ17) and psTPMT(Δ17)−sinefungin have been scaled, averaged, and mapped to a backbone ribbon diagram for the tertiary structure of the apoprotein in Figure 3 (numerical plots of the chemical shift differences are available as Supporting Information). The most dramatic changes are evident at the presumed SAM−sinefungin binding site, largely consisting of the loops and turns connecting β1−α1, β2−α2, β4−α4′, and, to a more limited extent, β3−α3. These residues surround a visible cleft in the protein structure located at the top and toward the center of the β-sheet, as viewed in Figure 3, which represents the highly conserved SAM-binding site found in the numerous crystallographic studies of classical methyltransferases (*11*). Additionally, sinefungin dramatically perturbs the chemical shifts of many residues apparently distal to this central site, likely representing *indirect* conformational effects of ligand binding on the protein. Note that β4 and

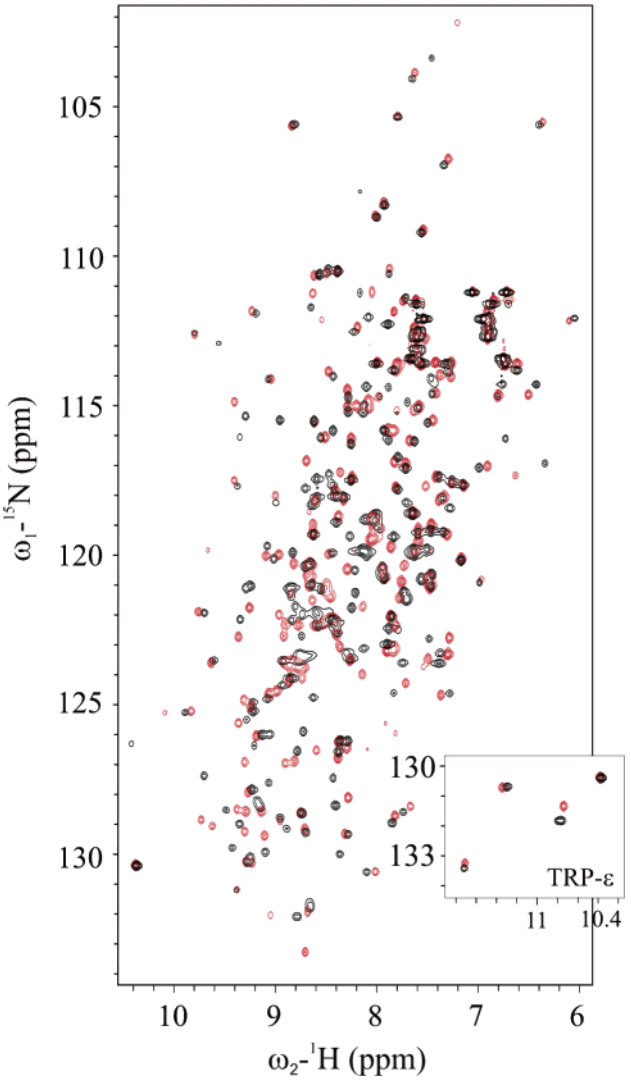

FIGURE 2: Superposed ^{1}H−^{15}N HSQC NMR spectra of uniformly ^{15}N-labeled 0.75 mM apo psTPMT (black) and 0.75 mM psTPMT−7.5 mM sinefugin (red).

α4′ represent the edge of the presumed SAM-binding site and all chemical shift changes beyond this point are considered distal. These indirect perturbations are generally located at the interface between the active site cover and the β-sheet, with the largest being evident at the top of β5 along with nearby residues in β7 and in the loop preceding α5. In fact, chemical shift changes extend all the way through α5 and into the loop before β6, located nearly on the opposite edge of the protein from the conserved SAM-binding site.

Missing psTPMT(Δ17) Resonances in the Presence of Sinefungin. Although nearly complete chemical shift assignments have been obtained for apo psTPMT(Δ17), numerous protein resonances cannot be identified after the addition of sinefungin despite extensive searching of many 2D and 3D NMR spectra collected at a variety of stoichiometric ratios of sinefungin to psTPMT(Δ17). These residues are colored gray in Figure 3 and cluster within the protein tertiary structure in a region adjacent to SAM−sinefungin that is also likely nearby the binding site for 6-TPs and the enzyme's active site. We offer two potential explanations for the loss of NMR signal for these residues. First, they may have become unstructured in the presence of sinefungin, allowing rapid exchange of their amide hydrogens with solvent and

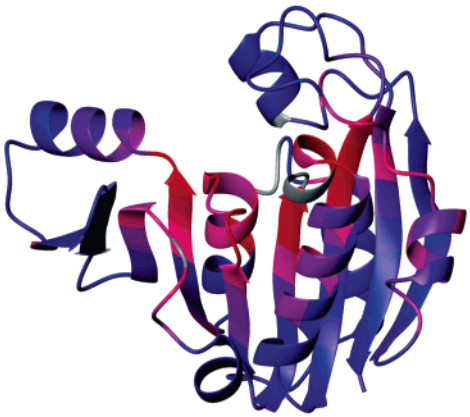

FIGURE 3: ^{1}H, ^{13}C, and ^{15}N NMR chemical shift differences between apo psTPMT and psTPMT−sinefungin are mapped onto a representative ribbon diagram of psTPMT. Chemical shift differences for H_N, N_H, Cα, Cβ, and CO of each residue expressed in hertz were summed and averaged over the number of assigned nuclei and finally displayed as a linear color gradient. Blue portions of the ribbon diagram represent sites of psTPMT unperturbed by sinefungin, while sites colored bright red represent the most dramatic chemical shift changes. Residues where H_N resonances were lost upon binding sinefungin are colored gray.

resulting in a loss of signal in the NMR experiments used for assignment of backbone resonances. Alternatively, the local chemical environment of these residues may be exchanging on a time scale similar to the corresponding differences in their chemical shifts, resulting in an apparent loss of NMR signal due to "exchange broadening". As these residues are presumably located in the vicinity of the chiral center in SAM and sinefungin described above, it is possible that stereochemical interconversion plays a role in this potential exchange reaction.

Comparison of NMR Relaxation Rates for Apo psTPMT-(Δ17) and psTPMT(Δ17)−Sinefungin. The R_1 and R_2 NMR relaxation rates and the steady-state ^{1}H→^{15}N NOE for the backbone amides of psTPMT(Δ17) in the presence and absence of sinefungin have been determined and plotted in Figure 4. Although an analysis of polypeptide backbone dynamics using the model-free formalism is presented below, a few notable features of the relaxation data are immediately apparent. As previously hypothesized from the solution structure of apo psTPMT(Δ17), the protein N-terminus is clearly structurally disordered as evidenced by dramatically elevated R_1 and depressed R_2 relaxation rates along with reduced steady-state ^{1}H→^{15}N NOE values for the first approximately four N-terminal residues. Additionally, binding of sinefungin uniformly increases R_1/R_2 relaxation rate ratios along the length of the polypeptide backbone, a finding most consistent with a small decrease in the *rate* of overall macromolecular tumbling upon binding ligand.

Model-Free Analysis. A description of the molecular dynamics along the polypeptide backbone has been extracted from the NMR relaxation data using the so-called "Lipari−Szabo" or "Modelfree" formalism (*36*, *37*), which has been extended multifold over the past two decades to account for anisotropic tumbling of the macromolecule (*38*, *39*), slower conformational exchange on the microsecond to millisecond time scale (*40*), and additional fast motions on the subpicosecond time scale (*41*, *42*). The most informative fruits of such analyses are the identification of unstructured regions, by their abundant fast motions on the nanosecond to

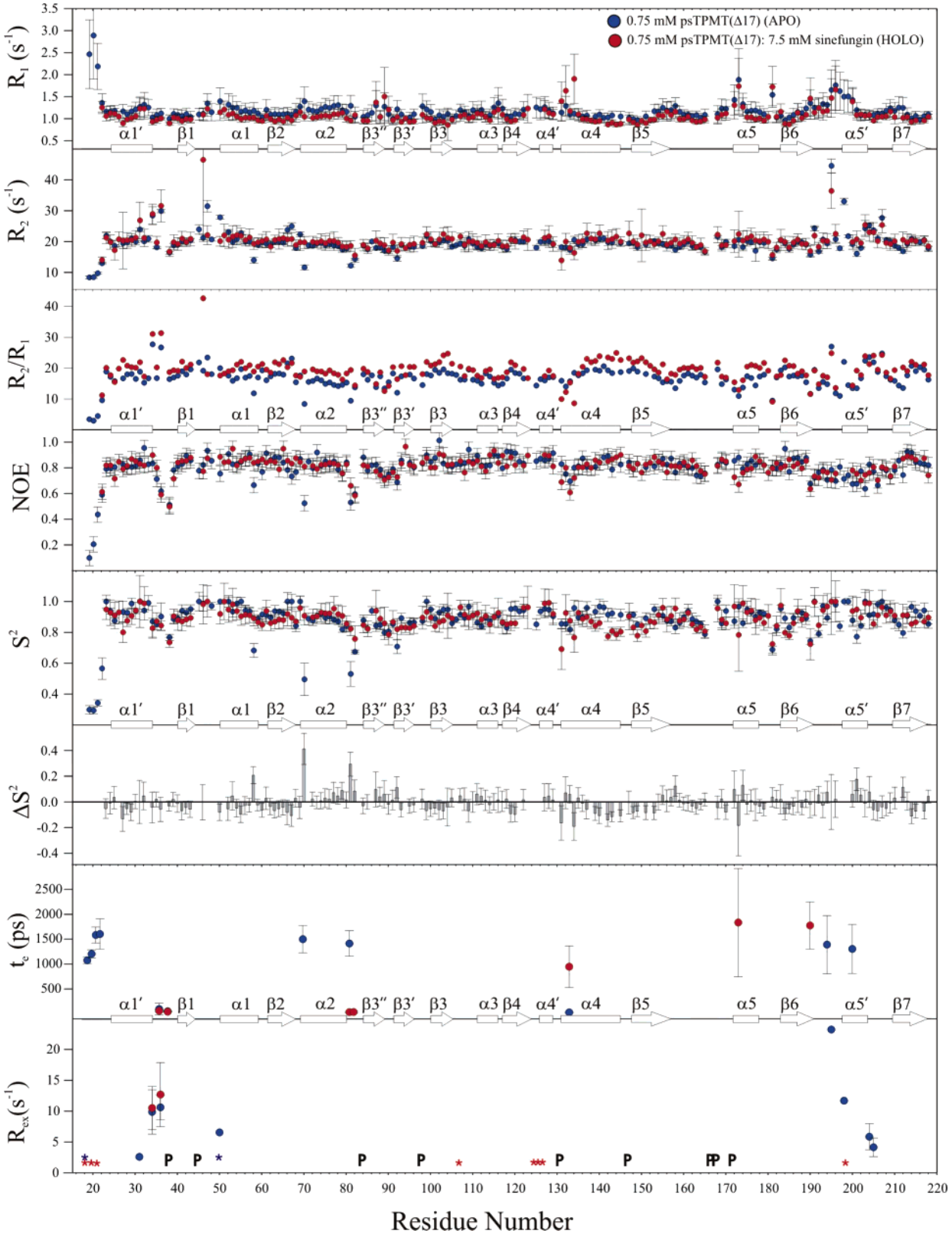

FIGURE 4: ^{15}N NMR relaxation data and corresponding model-free motional parameters for apo psTPMT (blue symbols) and psTPMT−sinefungin (red symbols) are plotted along the primary sequence of psTPMT, with the approximate location of secondary structure elements noted. Differences in the S^2 order parameter value are plotted to emphasize changes due to ligand binding, with negative values demonstrating an increase in flexibility and positive values indicating restricted mobility upon binding sinefungin. The locations of unassigned residues and proline residues are represented by asterisks and the letter P, respectively.

picosecond time scale, and regions displaying slower conformational exchange. Occurring on a time scale (microsecond to millisecond) more typical of biochemical processes such as ligand binding, protein−protein associations, and enzyme catalysis, conformational exchange often reveals functionally relevant protein motions. Both the liganded and unliganded states of psTPMT(Δ17) are best described by an isotropic model of rotational diffusion with overall

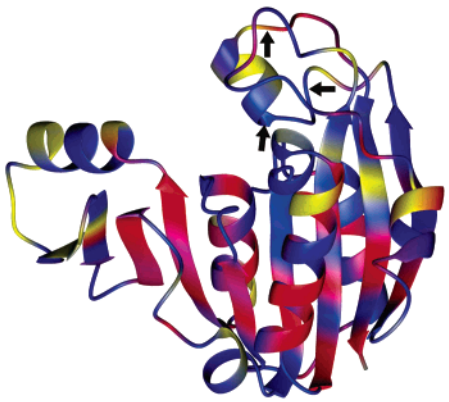

FIGURE 5: Differences in apo psTPMT and psTPMT−sinefungin order parameter (S^2) values are mapped onto the psTPMT tertiary structure. Residues with restricted mobility in psTPMT−sinefungin are plotted with a linear gradient between blue (no difference) and yellow ($0 \leq \Delta S^2 \leq 0.08$; everything over 0.08 colored bright yellow). Residues with increased mobility in the presence of sinefungin are similarly plotted with a color gradient from blue to red ($0 \geq \Delta S^2 \geq -0.08$). Sites where conformational exchange (R_{ex}) terms disappeared upon binding sinefungin are indicated by the arrows.

correlation times (τ_ms) of 14.0 and 13.3 ns, respectively. The internal mobility of individual residues has been illustrated in the bottom half of Figure 4 by variations in order parameters (S^2s), which are proportional to the amplitudes of fast time scale internal motions and range between 0 and 1 for fully unrestricted to fully restricted motions, respectively, and by the presence of conformational exchange terms (R_{ex}s), indicating slower time scale internal dynamics.

Summary of Internal Motions along the Polypeptide Backbone of Apo psTPMT(Δ17). In the absence of sinefungin, a majority of the protein backbone is well ordered, as evidenced by order parameters above approximately 0.8 and an absence of conformational exchange terms. However, besides the previously mentioned disordered N-terminus, three distinct foci of increased internal dynamics can be described: (1) The relatively lengthy loop stretching between α1′ and β1, located at the bottom of the protein structure as oriented in the figures, demonstrates mobility across a wide range of time scales by the presence of both lowered S^2 values and the presence of conformational exchange terms. (2) The inserted pair of antiparallel β-strands visible on the left edge of the protein structure, beginning with the C-terminal edge of α2 and extending all the way through strands β3″ and β3′, has increased mobility on the nanosecond to picosecond time scale with a number of S^2 values below 0.8. (3) The inserted structural element referred to as the active site cover, consisting of two extended loops between β5 and α5 and between β6 and β7, has complex internal dynamics, including scattered residues with significantly decreased S^2 values along with two pairs of residues, flanking each side of α5′, demonstrating slower time scale conformational exchange terms.

Changes in Polypeptide Backbone Dynamics upon Binding Sinefungin. To demonstrate the consequences of ligand binding on the fast time scale motions in psTPMT(Δ17), order parameter differences were plotted along the protein sequence in Figure 4 and mapped onto a backbone ribbon diagram of the protein structure in Figure 5, such that positive ΔS^2s indicating increased rigidity in the liganded state were rainbow colored from blue to yellow and negative ΔS^2s indicating increased mobility in the presence of sinefungin were rainbow colored from blue to red. Additionally, residues with evidence for changes in slower time scale motions, as evidenced by the loss of R_{ex} terms in the model-free analysis, are denoted in the figures. We note two distinct patterns for changes in polypeptide backbone dynamics of psTPMT(Δ17) upon binding sinefungin. (1) The central, conserved structural elements of the TPMT topology experience an increase in fast time scale motions when complexed with sinefungin, which is most evident along the length of β3, β2, β1, α1, and β4, along with the lower portions of α4, β5, β7, and β6. (2) In contrast, the peripheral, inserted/variable structural elements in the TPMT topology are conformationally stabilized by the presence of sinefungin. On the left edge of the protein structure, the inserted pair of antiparallel β-strands, β3″ and β3′, the associated α2 helix, and the loops between them have consistently higher order parameters in psTPMT(Δ17)−sinefungin compared to the apoprotein. Lastly, the set of inserted structural elements known as the active site cover is also stabilized by ligand. Previously noted conformational exchange terms for residues flanking each side of α5′ are lost upon binding sinefungin, indicating a decrease in slow time scale motions in this region. As well, order parameters (S^2s) for residues located throughout the active site cover, at its interface the central β-sheet and extending into the α5 helix, display varying perturbations due to ligand binding, which approximately correlate with chemical shift changes distal to the SAM−sinefungin binding site described above.

Structural Changes in the α4′ Minihelix. Binding of sinefungin dramatically perturbs the structural properties of residues in the vicinity of the α4′ minihelix. Centrally located between the presumed SAM and 6-TP binding sites, the α4′ minihelix displays significant chemical shift changes, missing resonance assignments, and higher order parameters in the presence of sinefungin. The chemical shift changes for the backbone resonances of these residues are uniformly consistent with a loss of helical secondary structure according to the principles of the CSI. The $H_N(i)-H_N(i+1)$ and $H_N(i)-H\alpha(i+3)$ NOEs characteristic of helices are not observed in the 3D ^{15}N-NOESYHSQC NMR spectrum collected on psTPMT(Δ17)−sinefungin but were previously readily identified for the apoprotein. Additionally, the amide hydrogens of these residues display fewer NOESY correlations in the presence of ligand compared to apo psTPMT(Δ17), with very different overall patterns of chemical shifts for the remaining NOESY cross-peaks, supporting a significant change in local chemical environment for these residues. Despite the apparent loss of helical secondary structure for these residues, their increase in order parameters without missing resonance assignments argues against an unstructured state in the presence of sinefungin. It is more likely that interaction with bound ligand has induced a localized conformational change for these residues, which will remain undefined until a detailed tertiary structure of psTPMT(Δ17) complexed with sinefungin has been determined. Of note, in the crystallographic structures of two other small molecule methyltransferases where the α4′ minihelix is present, its structure is intact and unperturbed by the SAM (*43*, *44*). Hence, the NMR spectroscopic changes for the α4′ minihelix in psTPMT may represent a novel structural perturbation or,

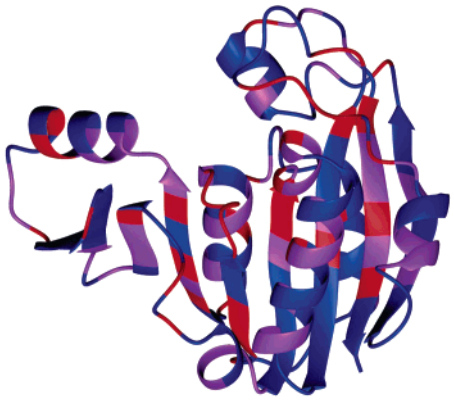

FIGURE 6: Conservation of the TPMT protein sequence established by ClustalW is mapped onto the tertiary structure of psTPMT. Residues invariant across the species are colored red in the figure, highly conserved residues are in purple, and the remaining residues are colored blue.

alternatively, a characteristic of the dynamic behavior of the protein in solution.

Sequence Conservation between Mammalian and Bacterial TPMTs. To compare the distribution of structural and dynamic changes in psTPMT(Δ17) with the evolutionary conservation of amino acids in the polypeptide backbone, a sequence alignment of five thiopurine methyltransferase protein sequences was mapped onto the protein structure in Figure 6. Strikingly, the location of invariant and highly conserved residues compares well with the mapping of chemical shift changes associated with binding sinefungin presented above in Figure 3. Many of the central residues expected to directly interact with SAM are either invariant or highly conserved. Additionally, many of the distal residues with *indirect* chemical shift changes upon binding sinefungin are also highly conserved evolutionarily in TPMT orthologues. However, comparisons of sequence homology with perturbations in backbone dynamics induced by sinefungin (Figure 5) are mixed. Residues in the central portion of the TPMT topology with increases in fast time scale mobility do not appear to correlate with patterns of sequence conversation. On the other hand, we note that residues in the active site cover whose dynamics are characterized by conformational exchange (R_{ex}) terms in the apoprotein, and are stabilized upon binding sinefungin, are either invariant (G204 and L205) or adjacent to highly conserved residues (L194 and R199) in the alignment. Similarly, on the other edge of the protein, residues in the α2 helix and the adjacent loop are both highly conserved in TPMT protein sequences and dynamically stabilized by sinefungin.

DISCUSSION

We have examined the consequences of binding sinefungin, a SAM analogue and general methyltransferase inhibitor, on the structural properties of psTPMT(Δ17) in aqueous solution using NMR spectroscopy. The overall pattern of complex effects is summarized in Figure 7 using a backbone ribbon diagram of the previously reported tertiary structure for apo psTPMT(Δ17). Colored red in the figure are the central structural elements with uniform increases in the amplitudes of fast time scale motions upon binding sinefungin. In contrast, peripheral structural features that appear conformationally stabilized by the presence of ligand are colored yellow. A combination of changes in backbone mobility and NMR chemical shifts in the active site cover, at its interface with the central β-sheet, and extending past α5 to the opposite edge of the protein, suggest the possibility of a concerted set of *indirect* conformational changes induced by sinefungin, which have been colored orange in the figure. Lastly, our analysis of NMR relaxation rates also indicates that psTPMT(Δ17)−sinefungin is perturbed on a global scale, as its solution tumbling behavior is that of a macromolecule slightly larger than the apoprotein, which could be explained either by an expansion of overall molecular volume, by an increase in the effective hydration shell, or by an increase in transient intermolecular interactions between monomers.

Ligand binding to protein is typically thought to feature enthalpy−entropy compensation, where a reduction in overall molecular entropy upon complexation is more than matched by enthalpic and entropic gains from the intermolecular interaction (*45*). Enthalpy is released by the favorable atomic interactions at the ligand binding site, including van der Waals contacts, hydrogen bonding, and electrostatic interactions, whereas entropic gains are classically considered to result from the release of ordered water molecules from the binding site, a phenomenon known as the hydrophobic effect. In many instances, association with ligand structurally stabilizes the protein, contributing additional enthalpic gains and entropic costs into the binding reaction. One of many examples is the disorder-to-order transition seen in the intestinal fatty acid-binding protein (*46*, *47*), in which a structurally disordered and protease-susceptible portion of the protein adopts a stable α-helical conformation upon binding fatty acid. Recent work has revealed an alternative scenario where entropic gains from ligand binding are due to widespread increases in mobility of the protein backbone (*48*−*52*). Binding of a small hydrophobic ligand in the internal cavity of major urinary protein-1 (MUP-1) is associated with widespread, though discontinuous, elevation of fast time scale backbone dynamics as monitored by NMR relaxation analysis. Similarly, 4-oxalocrotonate tautomerase (*53*), stromolysin (*54*), ribonuclease T1 (*55*), *E. coli* topoisomerase (*56*), and the AT-rich interaction domain of Mrf-2 (*57*) experience various degrees of elevated backbone mobility upon binding their respective ligands.

Analysis of the consequences of sinefungin binding on the structural properties of psTPMT(Δ17) reveals a combination of entropic effects. Sinefungin induces an increase in backbone mobility for the central structural elements in the protein in clear analogy to the results on proteins such as MUP-1, described above. In contrast, the peripheral structural elements are entropically stabilized by the presence of ligand. The functional implications of these complementary changes in backbone mobility are currently unclear and must await further study. However, as detailed below, we do speculate on the possibility of cooperativity between binding sinefungin and either the association reaction with substrate or the catalytic mechanism, either of which would involve conformational restriction of both the active site cover and its interface with the central β-sheet. Perhaps the entropic cost of decreased mobility in these specific regions is compensated by favorable increases in conformational entropy dispersed throughout the central portion of the tertiary structure.

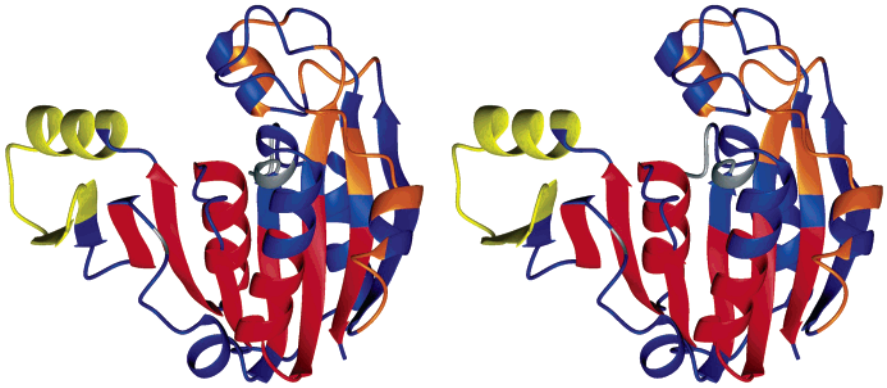

FIGURE 7: The overall patterns of structural and dynamic changes in the protein backbone of psTPMT upon binding sinefungin are color coded onto the ribbon diagram (presented in stereo). Conserved portions of the tertiary structure demonstrating consistent increases in fast time scale motions upon binding sinefungin are in red, peripheral structural elements that are conformationally stabilized by ligand are colored yellow, while those with little or no change are in blue. Residues colored orange display a combination of changes in both backbone dynamics and NMR chemical shifts distal to the SAM-binding site, suggesting the existence of indirect conformational changes in the enzyme possibly related to substrate recognition or the catalytic mechanism. Residues where H_N resonances were lost upon binding sinefungin are colored gray.

A semicontinuous pattern of dynamic stabilization and chemical shift perturbation, all in residues considered distal to the sinefungin recognition site, stretches from the active site cover to its interface with the central β-sheet and extends all the way through helix α5 to the opposite edge of the protein (colored orange in Figure 7). We speculate that a set of concerted structural changes occurring in these residues plays a role in catalysis, or at least promotes binding of substrate to the enzyme, in a fashion similar to the conclusions derived from an elegant series of biophysical studies performed on dihydrofolate reductase (DHFR) (*58*). Comparison of the static crystallographic structures (*59*−*65*) and the NMR-derived backbone mobilities (*66*, *67*) for three different ligation states of DHFR identified long-range motional couplings between structural changes in the active site and distal regions of the protein. Classical and hybrid quantum-classical molecular dynamics simulations of various DHFR complexes supported these findings by demonstrating large-scale conformational changes in the protein correlated with catalysis-promoting motions in the active site and also provided a mechanistic explanation for the dramatic effect of distal amino acid mutations on the rate of catalysis (*58*). Critical residues in this mechanism were highly conserved evolutionarily in DHFR orthologues. Although we do not have available a similar extensive set of biophysical studies to support our speculation of an analogous cooperative structural pathway involved in the enzymatic mechanism of psTPMT, which must await future research, we did identify a similar sequence conservation across TPMT orthologues for residues involved in our proposed set of long-range, concerted structural and dynamic changes in the protein backbone.

One of our major goals is to understand the structural mechanism for increased susceptibility of the polymorphic variants of human TPMT to intracellular degradation, and we are currently using the bacterial orthologue as a surrogate to investigate fundamental properties of the conserved TPMT tertiary structure. Mutants of psTPMT representing the clinically significant human polymorphisms are destabilized in solution similarly to the human enzyme (unpublished results). We are currently investigating the hypothesis that single residue polymorphisms in the protein sequence of TPMT redistribute the ensemble of conformations in solution away from the native structure toward a partially unstructured and dynamically fluctuating state. Protection from degradation afforded by SAM would be achieved by shifting the distribution of conformations away from the destabilized state by selectively binding to the native structure of the protein. Although the "wild-type" sequence of psTPMT investigated in the current study is not expected to populate the destabilized state to a significant degree, analysis of NMR relaxation may be sensitive to rare conformational fluctuations of the native structure and may uncover some structural features of the mechanism for polymorphic destabilization. Additionally, comparison of structural and dynamic properties for unliganded and liganded psTPMT will be valuable for future, planned studies on the polymorphic variants, where the structural fluctuations induced by the mutations will be identified by comparison to the current results.

We cautiously speculate that the present results may provide some insight into the structural mechanism by which SAM stabilizes the polymorphic mutants of TPMT. Binding of the SAM analogue, sinefungin, induces a widespread increase in backbone mobility for the core elements of the psTPMT topology. In a fashion similar to previous studies, we believe that the apo state of the protein is conformationally restricted by interaction of ordered solvent molecules with the unoccupied ligand binding site (*52*). Displacement of solvent by sinefungin relaxes the protein and allows a degree of flexibility in the backbone conformation. The degradation-susceptible polymorphisms in the TPMT protein sequence may be incompatible with the conformationally restricted apo state, because of unfavorable electrostatic or steric interactions, but better tolerated by the more relaxed and structurally flexible ligated protein.

The present work constitutes the first description of the polypeptide backbone dynamics of a classical, SAM-dependent methyltransferase. Despite the lack of sequence similarity, given the strong conservation of tertiary structure within this large family of proteins, the dynamic behavior of their polypeptide backbones may be shared as well. Of particular interest is the correlation of the patterns in backbone dynamics with the distribution of conserved and inserted/variable elements of the psTPMT topology. Similar

patterns in backbone mobility may be found in other small molecule methyltransferases, as they share similar structural insertions and variations in the consensus topology. We hypothesize that the dynamic behavior and structural changes in these inserted elements play a role in substrate recognition or the catalytic mechanism of TPMT and, potentially, for other small molecule methyltransferases. Lastly, genetic polymorphisms have been identified in additional methyltransferases (*68*−*74*), and although they are not as well characterized as those in TPMT, some of these appear to have both functional and clinical implications. Once again, we speculate that a general mechanism for destabilization of the conserved topology may be suggested by the current results, which are biologically utilized to generate genetic diversity in metabolic pathways in a fashion similar to TPMT and the metabolism of 6-TP medications.

ACKNOWLEDGMENT

J. Patrick Loria and Roger Cole are graciously acknowledged for helpful discussions and assistance with their FAST-Modelfree and sparky2rate software (http://xbeams.chem.yale.edu/∼loria/software.htm).

SUPPORTING INFORMATION AVAILABLE

NMR chemical shift assignments for psTPMT(Δ17)−sinefungin have been deposited in the BioMagResBank (http://www.bmrb.wisc.edu/) with the BMRB accession number 5886. Additional Supporting Information includes (1) chemical structures of SAM and sinefungin, (2) NMR spectral changes for representative residues during the sinefungin titration, (3) plots of NMR chemical shift differences between apo and psTPMT(Δ17)−sinefungin for all backbone and Cβ resonances, (4) a listing of amide ^{1}H and ^{15}N chemical shift changes for selected residues during the sinefungin titration, (5) a table of backbone amide NMR relaxation rates and Modelfree output, and (6) the ClustalW alignment of TPMT protein sequences. This material is available free of charge via the Internet at http://pubs.acs.org.

REFERENCES

1. Weinshilboum, R. (2001) Thiopurine pharmacogenetics: clinical and molecular studies of thiopurine methyltransferase, *Drug Metab. Dispos. 29*, 601−605.
2. Krynetski, E. Y., and Evans, W. E. (2000) Genetic polymorphism of thiopurine S-methyltransferase: molecular mechanisms and clinical importance, *Pharmacology 61*, 136−146.
3. Coulthard, S. A., and Hall, A. G. (2001) Recent advances in the pharmacogenomics of thiopurine methyltransferase, *Pharmacogenomics J. 1*, 254−261.
4. Weinshilboum, R. M., and Sladek, S. L. (1980) Mercaptopurine pharmacogenetics: monogenic inheritance of erythrocyte thiopurine methyltransferase activity, *Am. J. Hum. Genet. 32*, 651−662.
5. Lennard, L., Gibson, B. E., Nicole, T., and Lilleyman, J. S. (1993) Congenital thiopurine methyltransferase deficiency and 6-mercaptopurine toxicity during treatment for acute lymphoblastic leukaemia, *Arch. Dis. Child 69*, 577−579.
6. Evans, W. E., Horner, M., Chu, Y. Q., Kalwinsky, D., and Roberts, W. M. (1991) Altered mercaptopurine metabolism, toxic effects, and dosage requirement in a thiopurine methyltransferase-deficient child with acute lymphocytic leukemia, *J. Pediatr. 119*, 985−989.
7. Hernandez, J. S., Van Loon, J. A., Otterness, D. M., and Weinshilboum, R. M. (1990) Mouse thiopurine methyltransferase pharmacogenetics: correlation of immunoreactive protein and enzymatic activity, *J. Pharmacol. Exp. Ther. 252*, 568−573.
8. Tai, H. L., Fessing, M. Y., Bonten, E. J., Yanishevsky, Y., d'Azzo, A., Krynetski, E. Y., and Evans, W. E. (1999) Enhanced proteasomal degradation of mutant human thiopurine S-methyltransferase (TPMT) in mammalian cells: mechanism for TPMT protein deficiency inherited by TPMT*2, TPMT*3A, TPMT*3B or TPMT*3C, *Pharmacogenetics 9*, 641−650.
9. Tai, H. L., Krynetski, E. Y., Schuetz, E. G., Yanishevski, Y., and Evans, W. E. (1997) Enhanced proteolysis of thiopurine S-methyltransferase (TPMT) encoded by mutant alleles in humans (TPMT*3A, TPMT*2): mechanisms for the genetic polymorphism of TPMT activity, *Proc. Natl. Acad. Sci. U.S.A. 94*, 6444−6449.
10. Wang, L., Sullivan, W., Toft, D., and Weinshilboum, R. (2003) Thiopurine S-methyltransferase pharmacogenetics: chaperone protein association and allozyme degradation, *Pharmacogenetics 13*, 555−564.
11. Martin, J. L., and McMillan, F. M. (2002) SAM (dependent) I AM: the S-adenosylmethionine-dependent methyltransferase fold, *Curr. Opin. Struct. Biol. 12*, 783−793.
12. Scheuermann, T. H., Lolis, E., and Hodsdon, M. E. (2003) Tertiary structure of thiopurine methyltransferase from *Pseudomonas syringae*, a bacterial orthologue of a polymorphic, drug-metabolizing enzyme, *J. Mol. Biol. 333*, 573−585.
13. Koradi, R., Billeter, M., and Wuthrich, K. (1996) MOLMOL: A program for display and analysis of macromolecular structures, *J. Mol. Graphics 14*, 51−55.
14. Cournoyer, B., Watanabe, S., and Vivian, A. (1998) A tellurite-resistance genetic determinant from phytopathogenic pseudomonads encodes a thiopurine methyltransferase: evidence of a widely conserved family of methyltransferases, *Biochim. Biophys. Acta 1397*, 161−168.
15. Farrow, N. A., Muhandiram, R., Singer, A. U., Pascal, S. M., Kay, C. M., Gish, G., Shoelson, S. E., Pawson, T., Forman-Kay, J. D., and Kay, L. E. (1994) Backbone dynamics of a free and phosphopeptide-complexed Src homology 2 domain studied by 15N NMR relaxation, *Biochemistry 33*, 5984−6003.
16. Delaglio, F., Grzesiek, S., Vuister, G. W., Zhu, G., Pfeifer, J., and Bax, A. (1995) Nmrpipe—a multidimensional spectral processing system based on Unix pipes, *J. Biomol. NMR 6*, 277−293.
17. Kneller, D. G., and Goddard, T. D. (1997) University of California, San Francisco.
18. Mandel, A. M., Akke, M., and Palmer, A. G. (1995) Backbone dynamics of *Escherichia coli* ribonuclease Hi—Correlations with structure and function in an active enzyme, *J. Mol. Biol. 246*, 144−163.
19. Cole, R., and Loria, J. P. (2003) FAST-Modelfree: a program for rapid automated analysis of solution NMR spin-relaxation data, *J. Biomol. NMR 26*, 203−213.
20. Canet, D., Barthe, P., Mutzenhardt, P., and Roumestand, C. (2001) A comprehensive analysis of multifield ^{15}N relaxation parameters in proteins: determination of ^{15}N chemical shift anisotropies, *J. Am. Chem. Soc. 123*, 4567−4576.
21. Thompson, J. D., Higgins, D. G., and Gibson, T. J. (1994) CLUSTAL W: improving the sensitivity of progressive multiple sequence alignment through sequence weighting, position-specific gap penalties and weight matrix choice, *Nucleic Acids Res. 22*, 4673−4680.
22. Higgins, D. G., and Sharp, P. M. (1988) CLUSTAL: a package for performing multiple sequence alignment on a microcomputer, *Gene 73*, 237−244.
23. Ranjard, L., Prigent-Combaret, C., Nazaret, S., and Cournoyer, B. (2002) Methylation of inorganic and organic selenium by the bacterial thiopurine methyltransferase, *J. Bacteriol. 184*, 3146−3149.
24. Ranjard, L., Nazaret, S., and Cournoyer, B. (2003) Freshwater bacteria can methylate selenium through the thiopurine methyltransferase pathway, *Appl. Environ. Microbiol. 69*, 3784−3790.
25. Salavaggione, O. E., Yang, C., Kidd, L. B., Thomae, B. A., Pankratz, V. S., Trepanier, L. A., and Weinshilboum, R. M. (2004) Cat red blood cell thiopurine S-methyltransferase: companion animal pharmacogenetics, *J. Pharmacol. Exp. Ther. 308*, 617−626.
26. Casellas, P., and Jeanteur, P. (1978) Protein methylation in animal cells. I. Purification and properties of S-adenosyl-L-methionine: protein (arginine) *N*-methyltransferase from Krebs II ascites cells, *Biochim. Biophys. Acta 519*, 243−254.
27. Farooqui, J. Z., Tuck, M., and Paik, W. K. (1985) Purification and characterization of enzymes from *Euglena gracilis* that

methylate methionine and arginine residues of cytochrome *c*, *J. Biol. Chem. 260*, 537−545.
28. O'Dea, R. F., Pons, G., Hansen, J. A., and Mirkin, B. L. (1982) Characterization of protein carboxyl-O-methyltransferase in the spontaneous in vivo murine C-1300 neuroblastoma, *Cancer Res. 42*, 4433−4436.
29. Powell, L. M., Dryden, D. T., Willcock, D. F., Pain, R. H., and Murray, N. E. (1993) DNA recognition by the EcoK methyltransferase. The influence of DNA methylation and the cofactor S-adenosyl-L-methionine, *J. Mol. Biol. 234*, 60−71.
30. Schluckebier, G., Kozak, M., Bleimling, N., Weinhold, E., and Saenger, W. (1997) Differential binding of S-adenosylmethionine S-adenosylhomocysteine and sinefungin to the adenine-specific DNA methyltransferase M.TaqI, *J. Mol. Biol. 265*, 56−67.
31. Som, S., and Friedman, S. (1990) Direct photolabeling of the EcoRII methyltransferase with S-adenosyl-L-methionine, *J. Biol. Chem. 265*, 4278−4283.
32. Takata, Y., and Fujioka, M. (1992) Identification of a tyrosine residue in rat guanidinoacetate methyltransferase that is photolabeled with S-adenosyl-L-methionine, *Biochemistry 31*, 4369−4374.
33. Cannon, L. M., Butler, F. N., Wan, W., and Zhou, Z. S. (2002) A stereospecific colorimetric assay for (S,S)-adenosylmethionine quantification based on thiopurine methyltransferase-catalyzed thiol methylation, *Anal. Biochem. 308*, 358−363.
34. Hoffman, J. L. (1986) Chromatographic analysis of the chiral and covalent instability of S-adenosyl-L-methionine, *Biochemistry 25*, 4444−4449.
35. Wu, S. E., Huskey, W. P., Borchardt, R. T., and Schowen, R. L. (1983) Chiral instability at sulfur of S-adenosylmethionine, *Biochemistry 22*, 2828−2832.
36. Lipari, G., and Szabo, A. (1982) Model-free approach to the interpretation of nuclear magnetic-resonance relaxation in macromolecules. 2. Analysis of experimental results, *J. Am. Chem. Soc. 104*, 4559−4570.
37. Lipari, G., and Szabo, A. (1982) Model-free approach to the interpretation of nuclear magnetic-resonance relaxation in macromolecules. 1. Theory and range of validity, *J. Am. Chem. Soc. 104*, 4546−4559.
38. Schurr, J. M., Babcock, H. P., and Fujimoto, B. S. (1994) A test of the model-free formulas—Effects of anisotropic rotational diffusion and dimerization, *J. Magn. Reson., Ser. B 105*, 211−224.
39. Tjandra, N., Feller, S. E., Pastor, R. W., and Bax, A. (1995) Rotational diffusion anisotropy of human ubiquitin from N-15 NMR relaxation, *J. Am. Chem. Soc. 117*, 12562−12566.
40. Palmer, A. G., III, Kroenke, C. D., and Loria, J. P. (2001) Nuclear magnetic resonance methods for quantifying microsecond-to-millisecond motions in biological macromolecules, *Methods Enzymol. 339*, 204−238.
41. Clore, G. M., Driscoll, P. C., Wingfield, P. T., and Gronenborn, A. M. (1990) Analysis of the backbone dynamics of interleukin-1-beta using 2-dimensional inverse detected heteronuclear N-15-H-1 NMR spectroscopy, *Biochemistry 29*, 7387−7401.
42. Clore, G. M., Szabo, A., Bax, A., Kay, L. E., Driscoll, P. C., and Gronenborn, A. M. (1990) Deviations from the simple 2-parameter model-free approach to the interpretation of N-15 nuclear magnetic-relaxation of proteins, *J. Am. Chem. Soc. 112*, 4989−4991.
43. Martin, J. L., Begun, J., McLeish, M. J., Caine, J. M., and Grunewald, G. L. (2001) Getting the adrenaline going: crystal structure of the adrenaline-synthesizing enzyme PNMT, *Structure (Cambridge) 9*, 977−985.
44. Horton, J. R., Sawada, K., Nishibori, M., Zhang, X., and Cheng, X. (2001) Two polymorphic forms of human histamine methyltransferase: structural, thermal, and kinetic comparisons, *Structure (Cambridge) 9*, 837−849.
45. Stone, M. J. (2001) NMR relaxation studies of the role of conformational entropy in protein stability and ligand binding, *Acc. Chem. Res. 34*, 379−388.
46. Hodsdon, M. E., and Cistola, D. P. (1997) Discrete backbone disorder in the nuclear magnetic resonance structure of apo intestinal fatty acid-binding protein: implications for the mechanism of ligand entry, *Biochemistry 36*, 1450−1460.
47. Hodsdon, M. E., and Cistola, D. P. (1997) Ligand binding alters the backbone mobility of intestinal fatty acid-binding protein as monitored by ^{15}N NMR relaxation and ^{1}H exchange, *Biochemistry 36*, 2278−2290.
48. Krizova, H., Zidek, L., Stone, M. J., Novotny, M. V., and Sklenar, V. (2004) Temperature-dependent spectral density analysis applied to monitoring backbone dynamics of major urinary protein-I complexed with the pheromone 2-*sec*-butyl-4,5-dihydrothiazole, *J. Biomol. NMR 28*, 369−384.
49. Sharrow, S. D., Novotny, M. V., and Stone, M. J. (2003) Thermodynamic analysis of binding between mouse major urinary protein-I and the pheromone 2-*sec*-butyl-4,5-dihydrothiazole, *Biochemistry 42*, 6302−6309.
50. Sharrow, S. D., Vaughn, J. L., Zidek, L., Novotny, M. V., and Stone, M. J. (2002) Pheromone binding by polymorphic mouse major urinary proteins, *Protein Sci. 11*, 2247−2256.
51. Zidek, L., Stone, M. J., Lato, S. M., Pagel, M. D., Miao, Z., Ellington, A. D., and Novotny, M. V. (1999) NMR mapping of the recombinant mouse major urinary protein I binding site occupied by the pheromone 2-*sec*-butyl-4,5-dihydrothiazole, *Biochemistry 38*, 9850−9861.
52. Zidek, L., Novotny, M. V., and Stone, M. J. (1999) Increased protein backbone conformational entropy upon hydrophobic ligand binding, *Nat. Struct. Biol. 6*, 1118−1121.
53. Stivers, J. T., Abeygunawardana, C., and Mildvan, A. S. (1996) ^{15}N NMR relaxation studies of free and inhibitor-bound 4-oxalocrotonate tautomerase: backbone dynamics and entropy changes of an enzyme upon inhibitor binding, *Biochemistry 35*, 16036−16047.
54. Yuan, P., Marshall, V. P., Petzold, G. L., Poorman, R. A., and Stockman, B. J. (1999) Dynamics of stromelysin/inhibitor interactions studied by ^{15}N NMR relaxation measurements: comparison of ligand binding to the S1-S3 and S′1-S′3 subsites, *J. Biomol. NMR 15*, 55−64.
55. Fushman, D., Ohlenschlager, O., and Ruterjans, H. (1994) Determination of the backbone mobility of ribonuclease T1 and its 2′GMP complex using molecular dynamics simulations and NMR relaxation data, *J. Biomol. Struct. Dyn. 11*, 1377−1402.
56. Yu, L., Zhu, C. X., Tse-Dinh, Y. C., and Fesik, S. W. (1996) Backbone dynamics of the C-terminal domain of *Escherichia coli* topoisomerase I in the absence and presence of single-stranded DNA, *Biochemistry 35*, 9661−9666.
57. Zhu, L., Hu, J., Lin, D., Whitson, R., Itakura, K., and Chen, Y. (2001) Dynamics of the Mrf-2 DNA-binding domain free and in complex with DNA, *Biochemistry 40*, 9142−9150.
58. Agarwal, P. K., Billeter, S. R., Rajagopalan, P. T., Benkovic, S. J., and Hammes-Schiffer, S. (2002) Network of coupled promoting motions in enzyme catalysis, *Proc. Natl. Acad. Sci. U.S.A. 99*, 2794−2799.
59. Matthews, D. A., Alden, R. A., Bolin, J. T., Freer, S. T., Hamlin, R., Xuong, N., Kraut, J., Poe, M., Williams, M., and Hoogsteen, K. (1977) Dihydrofolate reductase: X-ray structure of the binary complex with methotrexate, *Science 197*, 452−455.
60. Matthews, D. A., Bolin, J. T., Burridge, J. M., Filman, D. J., Volz, K. W., Kaufman, B. T., Beddell, C. R., Champness, J. N., Stammers, D. K., and Kraut, J. (1985) Refined crystal structures of *Escherichia coli* and chicken liver dihydrofolate reductase containing bound trimethoprim, *J. Biol. Chem. 260*, 381−391.
61. Matthews, D. A., Bolin, J. T., Burridge, J. M., Filman, D. J., Volz, K. W., and Kraut, J. (1985) Dihydrofolate reductase. The stereochemistry of inhibitor selectivity, *J. Biol. Chem. 260*, 392−399.
62. Matthews, D. A., Alden, R. A., Bolin, J. T., Filman, D. J., Freer, S. T., Hamlin, R., Hol, W. G., Kisliuk, R. L., Pastore, E. J., Plante, L. T., Xuong, N., and Kraut, J. (1978) Dihydrofolate reductase from *Lactobacillus casei*. X-ray structure of the enzyme methotrexate·NADPH complex, *J. Biol. Chem. 253*, 6946−6954.
63. Bystroff, C., Oatley, S. J., and Kraut, J. (1990) Crystal structures of *Escherichia coli* dihydrofolate reductase: the $NADP^+$ holoenzyme and the folate·$NADP^+$ ternary complex. Substrate binding and a model for the transition state, *Biochemistry 29*, 3263−3277.
64. Davies, J. F., Jr., Delcamp, T. J., Prendergast, N. J., Ashford, V. A., Freisheim, J. H., and Kraut, J. (1990) Crystal structures of recombinant human dihydrofolate reductase complexed with folate and 5-deazafolate, *Biochemistry 29*, 9467−9479.
65. Bystroff, C., and Kraut, J. (1991) Crystal structure of unliganded *Escherichia coli* dihydrofolate reductase. Ligand-induced conformational changes and cooperativity in binding, *Biochemistry 30*, 2227−2239.
66. Osborne, M. J., Schnell, J., Benkovic, S. J., Dyson, H. J., and Wright, P. E. (2001) Backbone dynamics in dihydrofolate reductase complexes: role of loop flexibility in the catalytic mechanism, *Biochemistry 40*, 9846−9859.
67. Osborne, M. J., and Wright, P. E. (2001) Anisotropic rotational diffusion in model-free analysis for a ternary DHFR complex, *J. Biomol. NMR 19*, 209−230.

68. Shield, A. J., Thomae, B. A., Eckloff, B. W., Wieben, E. D., and Weinshilboum, R. M. (2004) Human catechol O-methyltransferase genetic variation: gene resequencing and functional characterization of variant allozymes, *Mol. Psychiatry 9*, 151−160.
69. Wang, L., Thomae, B., Eckloff, B., Wieben, E., and Weinshilboum, R. (2002) Human histamine *N*-methyltransferase pharmacogenetics: gene resequencing, promoter characterization, and functional studies of a common 5′-flanking region single nucleotide polymorphism (SNP), *Biochem. Pharmacol. 64*, 699−710.
70. Preuss, C. V., Wood, T. C., Szumlanski, C. L., Raftogianis, R. B., Otterness, D. M., Girard, B., Scott, M. C., and Weinshilboum, R. M. (1998) Human histamine *N*-methyltransferase pharmacogenetics: common genetic polymorphisms that alter activity, *Mol. Pharmacol. 53*, 708−717.
71. Weinshilboum, R. M., Otterness, D. M., and Szumlanski, C. L. (1999) Methylation pharmacogenetics: catechol O-methyltransferase, thiopurine methyltransferase, and histamine *N*-methyltransferase, *Annu. Rev. Pharmacol. Toxicol. 39*, 19−52.
72. Yan, L., Galinsky, R. E., Bernstein, J. A., Liggett, S. B., and Weinshilboum, R. M. (2000) Histamine *N*-methyltransferase pharmacogenetics: association of a common functional polymorphism with asthma, *Pharmacogenetics 10*, 261−266.
73. Yan, L., Szumlanski, C. L., Rice, S. R., Sobell, J. L., Lachman, H. M., and Weinshilboum, R. M. (2000) Histamine *N*-methyltransferase functional polymorphism: lack of association with schizophrenia, *Am. J. Med. Genet. 96*, 404−406.
74. David, C. L., Szumlanski, C. L., DeVry, C. G., Park-Hah, J. O., Clarke, S., Weinshilboum, R. M., and Aswad, D. W. (1997) Human erythrocyte protein L-isoaspartyl methyltransferase: heritability of basal activity and genetic polymorphism for thermal stability, *Arch. Biochem. Biophys. 346*, 277−286.

BI0492556